DOI: 10.1002/((please add manuscript number))

Article type: Communication

Magnetoelectric radical hydrocarbons

Ying-Shi Guan,[1,2,†] Guohua Zhong,[3,†] Yong Hu,[1,2,†] Anthony F. Cannella,[4] Changning Li,[1,2] Namhoon Lee,[1,2] Quanxi Jia,[5] David C. Lacy,[4,*] and Shenqiang Ren[1,2,*]

[1.] Department of Mechanical and Aerospace Engineering, University at Buffalo, The State University of New York, Buffalo, NY 14260

[2.] Research and Education in eNergy, Environment & Water (RENEW) Institute, University at Buffalo, The State University of New York, Buffalo, NY 14260

[3.] Shenzhen Institutes of Advanced Technology, Chinese Academy of Sciences, Shenzhen 518055, China.

[4.] Department of Chemistry, University at Buffalo, The State University of New York, Buffalo, NY 14260

[5.] Department of Materials Design and Innovation, University at Buffalo, The State University of New York, Buffalo, NY 14260

* Email: dclacy@buffalo.edu; shenren@buffalo.edu

† Y.-S. Guan, G. Zhong, and Y. Hu contributed equally to this work.

Abstract: The molecular radicals, systems with unpaired electrons of open-shell electronic structures, set the stage for a multidisciplinary science frontier relevant to the cooperative magnetic exchange interaction and magnetoelectric effect. Here we report ferroelectricity together with magnetic spin exchange coupling in molecular radical hydrocarbon solids, representing a new class of magnetoelectrics. Electronic correlation through radical-radical interactions plays a decisive role in the coupling between magnetic and charge orders. We find a substantial photoconductance and visible-light photovoltaic effect in radical hydrocarbons. The ability to simultaneously control and retrieve the changes in magnetic and electrical responses opens up a new breadth of applications, such as radical magnetoelectrics, magnets, and optoelectronics.

Recently, there has been a growing interest in the study of organic radical materials with unpaired electrons of open-shell electronic structures that exhibit electronic cooperative interactions.[1-7] Molecular radicals are an especially interesting condensed matter associated with the atomic center in a molecule, where the weak unpaired electron interactions can lead to a macroscopically characteristic state in bulk assemblies (high-temperature molecular magnet, superconductor, etc). Recent investigations of molecular radicals have mainly concentrated on the exchange interaction involving s and p orbitals. For a pair of correlated electrons in different orbitals, the net spin (S) can be either 0 (antiparallel spins) or 1 (parallel spins), corresponding to the singlet and triplet states, which can attribute to the antiferromagnetic or ferromagnetic spin coupling.[4-6] If such significant coupling can be maintained in a crystalline extended bulk structure, molecular radical magnets with high Curie or Neel temperature could be achievable. Although considerable progress has been made in the preparation of molecular radical magnets, the design of all-molecular radical magnetoelectric materials (RMEs) has remained elusive.[8-12] The prominent magnetoelectric mechanisms of organics include the spin and charge-order driven ferroelectricity in quantum antiferromagnetic compounds.[12-14]

The RMEs provide an efficient method for the mutual control of radical magnetism and electric dipoles. The coupling between the magnetic and the electric orders generates novel functionalities, which do not exist in either single state[8,9,15-17]. In recent years there has been an enormous effort to discover new classes of polycyclic aromatic hydrocarbons (PAHs) with two or more functionalities, for example, magnetism[3-5] and conductivity[18], ferroelectricity and optoelectronics[19,20], which is partially associated with complex charge-transfer and radical interactions. The relationship between magnetic order characteristics and charge order has rarely been studied in PAHs, which is distinctly different from the typical ME effect in inorganic materials,[12,15] especially the inorganic single solid phase with magnetoelectric effect [21-22]. Radical magnetic interactions in PAHs rely on the competition between the spins of unpaired electrons and thermal motion, and therefore, diradicals with magnetic exchange interactions are particularly relevant as they are comparable to thermal energy kT within the available temperature range. In addition, utilization of charge-transfer and radical PAHs with large visible-light absorption is a promising route toward photoconductance and photovoltaic applications.[23]

Here we investigate potassium-doped radical terphenyl ($K_{1.5}C_{18}H_{14}$) PAH with bulk antiferromagnetic spin coupling and ferroelectric imidazolium perchlorate ($ImClO_4$) compound RME solids, where the K atom is between two $C_{18}H_{14}$ layers along the a-axis direction for the herringbone structured $K_{1.5}C_{18}H_{14}$,[22] and $ImClO_4$ with highly oriented (2,-1,0) and (1,0,-2) variants belongs to noncentrosymmetric R3m space group. By chemical means with highly reactive potassium alkali metal, $C_{18}H_{14}$ is capable of forming radical ($C_{18}H_{13}^{\cdot}$). The Raman and electronic absorption spectra are applied to study the radical terphenyl response to the magnetic and electric orders as well as their coupling behaviors. The importance of K dopant ratio on the magnetic interactions of $K_{1.5}C_{18}H_{14}$ has been pointed out with the antiferromagnetic coupling ground state.[24] $ImClO_4$ becomes ferroelectric below 373 K with the piezoelectric coefficient d_{33} of 41 pC/N, among the highest in molecular ferroelectrics.[25] We find that in $K_{1.5}C_{18}H_{14}$-$ImClO_4$ (K-Im) RME compounds, there exist a substantial photoconductance and visible-light photovoltaic effect and depend strongly on the intensity of light illumination. We also show that the correlation between the ferroelectric and magnetic orders of the $ImClO_4$ and K-terphenyl plays a decisive role in the coupling of radical, magnetic, and charge orders as evident in the simultaneously involving resistivity, dielectric constant, and magnetic coupling at a transition temperature of ~250 K.

The individual $K_{1.5}C_{18}H_{14}$ and $ImClO_4$ compounds are prepared via solid state sintering and liquid phase assembly, respectively. The solid composite $K_{1.5}C_{18}H_{14}$-$ImClO_4$ pellet is then prepared by pressing the uniformly mixed powder of $K_{1.5}C_{18}H_{14}$ and $ImClO_4$ (Figure 1a). The properties of the composites will be described further later. First, we show the Raman spectrum of the radical molecular $K_{1.5}C_{18}H_{14}$ compound (Figure 1b). The bands observed at 1001 and 776 cm^{-1} indicate the significant contribution from the modes of the terminal rings. The 1320 cm^{-1} band can be assigned to the inter-ring C-C stretching vibration. The bands in the 910-1120 cm^{-1} regions are the C-H bending vibration. Furthermore, the ICP-MS analysis of the samples $K_{1.5}C_{18}H_{14}$ confirmed that $K_{1.5}C_{18}H_{14}$ have a potassium content consistent with 1.5 potassium ions for every p-terphenyl. Figure 1c shows the SEM images of $ImClO_4$ with highly oriented (2,-1,0) and (1,0,-2) variants belongs to noncentrosymmetric R3m space group (Figure 1d). The morphology of the high density and closely packed composite K-Im pellet is investigated using scanning electron microscopy (Figure 2a), where the EDS mapping confirms the uniform C, K, Cl and N elemental distribution throughout the K-Im composite, which is critical for a highly electronic correlated material system. The K-Im samples with a weight ratio of 3:1, 2:1, 1:1, 1:2 and 1:3 between $K_{1.5}C_{18}H_{14}$ and $ImClO_4$ are also prepared for the further studies (Figure S1). To corroborate our interpretation, we perform complementary scanning force microscopy studies on the pellet samples. The surface potential image of K-Im composites with a weight ratio of 1:2 shows well-defined or distinguished two phases (Figure 2b), where the contact potential difference implies the existence of conducting $K_{1.5}C_{18}H_{14}$ and non-conducting $ImClO_4$ regions. The existence of ferroelectric $ImClO_4$ phase is further confirmed by the domain switching via piezoresponse force microscopy (PFM) illustrated in Figure 2c-2d. The distinct domain switching corroborates the ferroelectric polarization in $ImClO_4$ as a function of cyclic writing voltage. The piezoresponse hysteresis loop shows the switchable in-plane polarization of $ImClO_4$ (Figure S2).

The formation of radicals in the molecular $K_{1.5}C_{18}H_{14}$ compound is further confirmed by electron paramagnetic resonance (EPR) spectroscopy. The EPR spectra of the molecular $K_{1.5}C_{18}H_{14}$ compound exhibit a classic Lorentzian shape with an isotropic signal centered at g = 2.0029 at room temperature. In addition, the EPR signal at 77 K displayed partially resolved hyperfine structure, indicating the radical interactions at low temperature (Figure 3a). The molecular $K_{1.5}C_{18}H_{14}$ compound is also characterized using attenuated total reflectance Fourier transform infrared (ATR-FTIR) spectroscopy (Figure 3b), confirming that the p-terphenyl backbone is intact. This is evidenced by the presence of C–C stretching at ~1500 cm^{-1} and C–H stretching at ~3000 cm^{-1}, which is in good agreement with the Raman data. The absorption spectrum of $K_{1.5}C_{18}H_{14}$ shown in Figure 3c is closely related to the electronic transition features of the material, where the bands observed in the visible and near-infrared region (572-940 nm) can be attributed to the terphenyl radical.[26] Furthermore, we have investigated the magnetic structure of $K_{1.5}C_{18}H_{14}$ by employing the first-principles calculations within the framework of the vdW-DF2 functional.[27] $K_{1.5}C_{18}H_{14}$ is stabilized at *P*1 symmetry with crystal lattice parameters of *a* = 7.110 Å, *b* = 7.274 Å, *c* = 14.743 Å, the angle *α*=89.756, *β*=64.559 and *γ*=90.021, respectively. Three possible magnetic configurations were considered, including the non-magnetic (NM) state without spin polarization, the ferromagnetic (FM) state, and the antiferromagnetic (AFM) state. By calculating total energies at different magnetic states, we found that the total energy of AFM state is -456.14978 eV which is 9.2 meV and 1.8 meV less than those of NM and FM states under ambient pressure, respectively. The result indicates that K1.5C18H14 is stabilized at the AFM ground-state. Figure 3d shows the AFM spin polarization where the different colors of electronic clouds represent the difference of spin directions. The local spin magnetic moment is about 0.23 μB/f.u.

A photocurrent can be induced in the K-Im composite under light illumination. The photovoltaic effect has been studied in such molecular charge-transfer and radical hydrocarbons. The observed diode-like behavior of K-Im composites suggests its possibility of a photovoltaic effect, while the measurable photoconduction occurs with light illumination with a maximum photoconductivity of 0.2 S/cm (Figure 4a), which could result from the formation of radical percolation networks for electronic communications. The photocurrent gradually increased with the increase of light intensity, consistent with an increase in the density of charge carriers. As a control, the photoresponse of the $ImClO_4$ and $K_{1.5}C_{18}H_{14}$ were investigated, but they both exhibited subtle photoresponse (Figure S3). When the K-Im is held at open-circuit and excited by photoillumination, the resulting photovoltage is shown in Figure 4b. In the dark, there are no photocarriers present corresponding to the zero photovoltage. During the light on phase, the exciton generation in the hydrocarbon undergoes the charge transfer at the interface to generate photocarriers. The accumulation of photocarriers generates the linear photovoltage under the light intensity dependence, while the photovoltage plateau is observed before a substantial recombination. Figure S4 shows the time-dependent photocurrent at zero bias in K-Im solids with the turning of light on and off.

Our hypothesis is that the photoresponse results from the coupling of the ferroelectric ImClO4 phase and charge-transfer radical $K_{1.5}C_{18}H_{14}$ phase. Because the divergence of the polarization is equivalent to a distribution of bound charges, interfaces between two phases are likely to accumulate a local excess of charges. In particular, bound charges tend to accumulate at interfaces. When an electric field is applied, the dipoles in ferroelectric phase $ImClO_4$ can align orderly, generating polarization field at the interfaces between two phases. The polarization field provided by $ImClO_4$ can facilitate the separation of the photogenerated exciton. Therefore, the efficient separation of holes and electrons leads to the dramatically increased photocurrent due to the electric field poling effect. The existence of the ferroelectric phase plays an important role in the high photoresponse of the K-Im solids. The thermal variation induced current and pyroelectric current induced by the light illumination can be ruled out due to its transient nature (see Figure S4), while the steady photocurrent is observed from the photovoltaic effect of ferroelectric facilitated molecular hydrocarbons. Radicals in hydrocarbons are central to its conductivity and magnetic characteristics. The spin transport resulting from radical formation in the presence of an external magnetic field dictates the transport behavior of K-Im solids (Figure S5). A positive conductivity effect is observed in magneto-conductance, demonstrating that the external magnetic field can effect on the radical population. The external magnetic field can induce intersystem crossing between singlet and triplet radicals states. The ratio of singlet and triplet radicals can be influence by the competition between the spin-conserving through spin-exchange interaction and the spin-mixing caused by the external magneticfield. This change induces a chemical potential splitting between the spin-mixing and spin-conserving in K-Im, particularly a higher chemical potential of radicals leading to a smaller activation energy and positive conductivity effect. Photoillumination causes the radical population to increase for an improved positive conductivity under the magnetic field effect (Figure S6); this might indicate an antiferromagnetic to ferromagnetic coupling transition, or lowering a barrier for spin-frustrated radicals to propagate.

In order to gain information on the conductance of K-Im solids, we have performed standard temperature dependent four-point probe resistivity measurement as shown in Figure 5a. The resistivity is approximately 2.2 $x10^5$ Ω cm at 300 K, while a transition occurs at a temperature centered around 250 K. No drastic change is observed when the sample is cooled down further to 150 K (the measured range we have carried out). The conductivity changes by one order of magnitude across the transition region, while the band gap decreases. It is interesting to note that the transition observed in K-Im solid, where charge or spin ordering might be of relevance due to the radical-radical interaction with the decrease of temperature. In this material, we envision net antiferromagnetic coupling between the molecular radicals. However, there are also "spin-frustrated" edge radicals that couple to nearby antiferromagnetically coupled bi-radical systems. It is this spin that transports through the material. A transition occurs at 250 K (Figure 5b) that increases the radical mobility through the solid, possibly indicating a change in magnetic properties the enable a greater spin mobility - although the exact nature of these properties are unknown at this stage.

Comprehensive magnetic investigations are under way to clarify the magnetic ground state in $K_{1.5}C_{18}H_{14}$. Note that no noticeable structural change of both $ImClO_4$ and $K_{1.5}C_{18}H_{14}$ around 250 K further suggests that the anomaly of resistivity and magnetization around 250 K is a result of magnetic-electric order interactions. The temperature behavior of dielectric properties of K-Im composite is shown in Figure 5c at different frequencies at the similar temperature region. The anomaly of the dielectric constant around 250 K is in good agreement with the temperature dependent resistivity and magnetization measurements. Collectively, these concurrent changes in properties around the same temperature suggest that the magneto-electric coupling in $K_{1.5}C_{18}H_{14}$ and $ImClO_4$ plays a critical role in the magnetic and electric properties of the composites. The nature of this correlation is uncertain by we hypothesize that there is a direct coupling between magnetic and charge orders.

The temperature dependent magnetization measurement revealed an apparent anomaly of magnetization in K-Im at the ferroelectric transition temperature Tc ~ 373 K of $ImClO_4$ through measuring the magnetization in the temperature range 300K-420K (Figure 6a). At ferroelectric transition, a distinct rise in the magnetization of ~ $4x10^{-5}$ emu/g is observed, which is 14% of magnetization at 1000 Oe magnetic field. The pronounced dielectric peak of $ImClO_4$ phase suggests the ordering of electric dipoles below the order-disorder transition (Tc ~ 373 K), while the accumulated charge orders result in an enhancement of the moment, as we observed in the temperature dependent magnetization measurement. Furthermore, tuning and controlling magnetization of K-Im are performed by applying external electric field as a function of time at room temperature (Figure 6b). When an electric field is applied on the sample, the radical density is increased which in turn affects the magnetic exchange interaction with a magnetoelectric coupling coefficient ME_E= ~2.9 V/Oe cm.[28] To further investigate the coupling of the magnetic and electric order parameters, the pressure-dependent magnetization measurements through uniaxial compression was carried out as a function of temperature. As shown in Figure S7, the magnetization of the composite sample is apparently enhanced by applying an external pressure. This is reasonable considering that the piezoelectric property of the $ImClO_4$. The uniaxial pressure can induce charges in $ImClO_4$ that could be coupled to radicals, which in turn tunes the magnetization of $K_{1.5}C_{18}H_{14}$.

In summary, we demonstrate electric and magnetic coupling, and photovoltaic effects in the molecular radical hydrocarbons. The interplays among resistivity, dielectric, and magnetic spin properties of K-Im RMEs suggest the formation of organic magnetoelectric solid by forming molecular ferroelectric and radical hydrocarbon composites. We demonstrate that the magnetic and charge orders are directly coupled to one another as evidenced by the temperature dependent magneto/electronic properties. This finding represents a step forward in understanding and exploiting magnetoelectric effects in organic molecular radical hydrocarbons.

Supporting Information

Supporting Information is available from the Wiley Online Library or from the author.

Acknowledgements

Y.-S. Guan, G. Zhong, and Y. Hu contributed equally to this work. The U.S. Department of Energy, Office of Basic Energy Sciences, Division of Materials Sciences and Engineering supports S.R. under Award DE-SC0018631 (Magnetoelectrics). Financial support was provided by the U.S. Army Research Office supports S.R. under Award W911NF-18-2-0202 (Materials-by-Design and Molecular

Assembly). ICP-MS (NSF MRI CHE-0959565) was completed at the UB Chemistry Instrument Center, University at Buffalo, SUNY, Buffalo, NY.

Received: ((will be filled in by the editorial staff))
Revised: ((will be filled in by the editorial staff))
Published online: ((will be filled in by the editorial staff))

References

[1] G. E. Rudebusch, J. L. Zafra, K. Jorner, K. Fukuda, J. L.Marshall, I. Arrechea-Marcos, G. L. Espejo, R. P. Ortiz, C. J. Gomez-Garcia, L. N. Zakharov, M. Nakano, H. Ottosson, J. Casado, M. M. Haley. *Nat. Chem.* **2016,** *8*, 753.

[2] Y. Joo, V. Agarkar, S. H. Sung, B. M. Savoie, B. W. Boudouris. *Science* **2018,** *359*, 1391.

[3] S. Lee, F. Miao, H. Phan, T. S. Herng, J. Ding, J. Wu, D. Kim. *ChemPhysChem.* **2017**, *18,* 591.

[4] K. Kamada, K. Ohta, A. Shimizu, T. Kubo, R. Kishi, H. Takahashi, E. Botek, B. Champagne, M. Nakano. *J. Phys. Chem. Lett.* **2010,** *1 (6)*, 937.

[5] M. Ishida, J.-Y. Shin, J. M. Lim, B.S. Lee, M.-C. Yoon, T. Koide, J. L. Sessler, A. Osuka, D. Kim. *J. Am. Chem. Soc.* **2011,** *133,* 15533.

[6] A. Rajca, J. Wongsriratanakul, S. Rajca, *Science* **2001,** *294,* 1503.

[7] Z. Zeng, X. Shi, C. Chi, J. T. L. Navarrete, J. Casado, J. Wu. *Chem. Soc. Rev.*, **2015,** *44,* 6578.

[8] W. Eerenstein, N. D. Mathur, J. F. Scott. *Nature,* **2006,** *442,* 759.

[9] F. Kagawa, S. Horiuchi, M. Tokunaga, J. Fujioka, Y. Tokura. *Nat. Phys.* **2010,** *6,* 169.

[10] D. W. Fu, W. Zhang, H.-L. Cai, Y. Zhang, J.-Z. Ge. R.-G. Xiong, S. D. Huang, T. Nakamura. *Angew. Chem. Int. Ed.* **2011,** *50,* 11947.

[11] P. Lunkenheimer, J. Muller, S. Krohns, F. Schrettle, A. Loidl, B. Hartmann, R. Rommel, M. Souza, C. Hotta, J. A. Schlueter, M. Lang. *Nat. Mater.* **2012,** *11,* 755.

[12] M. Fiebig, T. Lottermoser, D. Meier, M. Trassin, *Nat. Rev. Mater.* **2016,** *1,* 16046.

[13] F. Matsukura, Y. Tokura, H. Ohno. Nat. Nanotech. **2015,** *10,* 209.

[14] Z. Tu, M. Wu, X. C. Zeng. *J. Phys. Chem. Lett.* **2017,** *8*, 1973.

[15] H. Zheng, J. Wang, S.E. Lofland, Z. Ma, L. Mohaddes-Ardabili, T. Zhao, L. Salamanca-Riba, S. R. Shinde, S. B. Ogale, F. Bai, D. Viehland, Y. Jia, D. G. Schlom, M. Wuttig, A. Roytburd, R. Ramesh. *Science* **2004,** *303,* 661. .

[16] D. Khomskii. *Physics* **2009,** *2*, id. 20.

[17] G. C. Xu, W. Zhang, X.-M. Ma, Y.-H. Chen, L. Zhang, H.-L. Cai, Z.-M. Wang, R.-G. Xiong, S. Gao. *J. Am. Chem. Soc.* **2011,** *133,* 14948.

[18] G. Lin, Y. Qin, Y.-S. Guan, H. Xu, W. Xu, D. Zhu. *RSC Adv.* **2016,** *6,* 4872.

[19] Y. S. Guan, Y. Qin, Y. Sun, C. Wang, W. Xu, D. Zhu. Chem. Commun. **2015,** *51,* 12182.

[20] Y. S. Guan, Y. Qin, Y. Sun, J, Chen. Xu, D. Zhu. Chem. Commun. **2016,** *52,* 4648.

[21] H. –L. Cai, Y. Zhang, D.-W. Fu, W. Zhang, T. Liu, H. Yoshikawa, K. Awaga, R.-G. Xiong. *J. Am. Chem. Soc.* **2012,** *134*, 18487.

[22] Y. Zhang, W.-Q. Liao, D.-W. Fu, H. –Y. Ye, C.-M. Liu, Z.-N. Chen. R.-G. Xiong. *Adv . Mater.* **2015,** *27,* 3942.

[23] D. Ellsworth, L. Lu, J. Lan, H. Chang, P. Li, Z. Wang, J. Hu, B. Johnson, Y. Bian, J. Xiao, R. Wu, M. Wu. *Nat. Phys.* **2016,** *12,* 861.

[24] G.-H. Zhong, X.-H. Wang, R.-S. Wang, J.-X. Han, C. Zhang, X.-J. Chen, H.-Q. Lin. *J. Phys. Chem. C,* **2018,** *122,* 3801.

[25] Y. Zhang, Y. Liu, H.-Y. Ye, D.-W, Fu, W. Gao, H. Ma, Z. Liu, Y. Liu, W. Zhang, J. Li. *Angew. Chem. Int. Ed.* **2014,** *53,* 5064.

[26] Y. Furukawa, H. Ohtsuka, M. Tasumi. Synth. Met. **1993**, *55-57,* 516-523.

[27] G.-H. Zhong, C. Zhang, X. Yan, X. Li, Z. Du, G. Jing, C. Ma. *Mol. Phys.* **2017,** *115 (4)*, 472.

[28] M. Vopsaroiu, M. Stewart, T. Hegarty, A. Muniz-Piniella, N. McCartney, M. Cain, G. Srinivasan. *Meas. Sci. Technol.* **2008**, *19,* 045106.

Figure captions

Figure 1 | Fabrication of K-Im. (a) The schematic diagram for the preparation of K-Im composite. (b) The Raman spectrum of $K_{1.5}C_{18}H_{14}$. Inset: the photograph of K-terphenyl pellet. (c) The scanning electron microscopy (SEM) image of the $ImClO_4$ crystals. (d) The X-ray diffraction (XRD) pattern of $ImClO_4$ crystals. Inset: the photograph of $ImClO_4$ crystal.

Figure 2 | The structural characterization of K-Im. (a) The SEM images and energy dispersive spectroscopy (EDS) mapping of K-Im composite with K-terphenyl:Im =1:2. (b) The conducting atomic force microscopy (AFM) of K-Im composite with K-terphenyl:Im =1:2. (c-d) Piezoresponse force microscopy (PFM) phase and amplitude mapping images of the K-Im composite with K-terphenyl:Im =1:2.

Figure 3 | The Charcterization of K-terphenyl radical. (a) The electron paramagnetic resonance (EPR) spectra of the $K_{1.5}C_{18}H_{14}$ at room temperature (298K) and 77K. (b) The fourier-transform infrared spectroscopy (FTIR) spectrum of the $K_{1.5}C_{18}H_{14}$. (c) The UV-Vis absorption spectrum of the $K_{1.5}C_{18}H_{14}$. (d) The calculated spin polarization for $K_{1.5}C_{18}H_{14}$, different colors of electronic clouds represent the difference of spin directions. Iso-surface unit: 2×10^{-3} e/Å^3.

Figure 4 | The light-induced electronic properties of K-Im. (a) The current-voltage (I-V) curves of the K-Im composite with K-terphenyl:Im =1:2, under light illumination with different intensities. (b) The time dependent photo-voltage generated under light illumination with the intensity of 40 mW/cm^2.

Figure 5 | The charge and spin order coupling in K-Im. (a) The temperature dependent resistivity of the K-Im composite with K-terphenyl:Im =1:2. (b) The temperature dependent magnetization of the K-Im composite with K-terphenyl:Im =1:2. (c) The temperature-dependent dielectric constant of K-Im composite with K-terphenyl:Im =1:2.

Figure 6 | The magnetoelectric coupling in K-Im. (a) The temperature dependent magnetization of the K-Im composite with K-terphenyl:Im =1:2 and the differential scanning calorimetry (DSC) curve of $ImClO_4$. (b) The electrically induced magnetic switching, under external electric field.

Figure 1

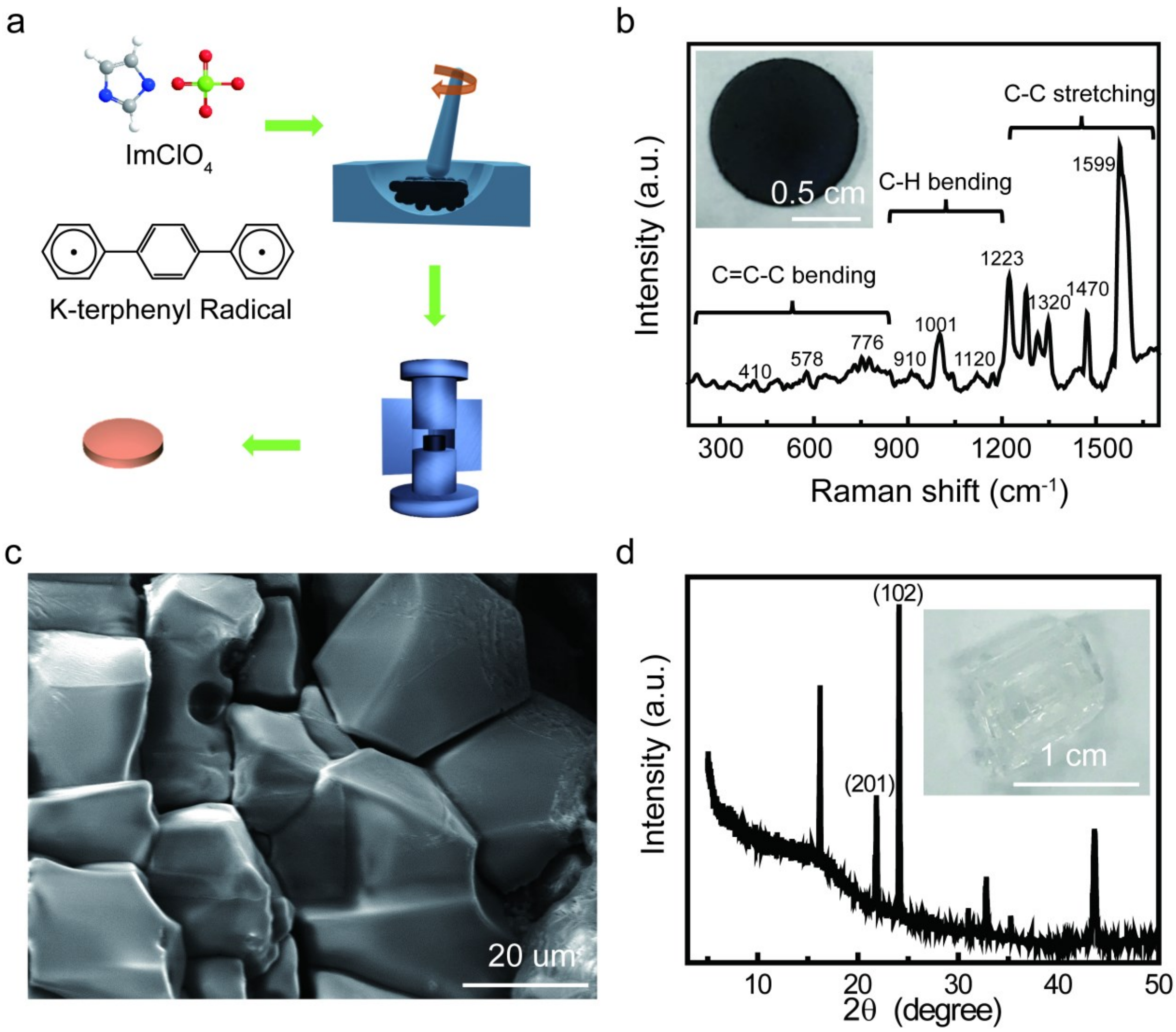
a
$ImClO_4$
K-terphenyl Radical
b
Intensity (a.u.)
0.5 cm
C-C stretching
C-H bending
C=C-C bending
1599
1223
1470
1320
1001
776
578
410
910
1120
300
600
900
1200
1500
Raman shift (cm^{-1})
c
20 um
d
Intensity (a.u.)
(102)
(201)
1 cm
10
20
30
40
50
2θ (degree)

Figure 2

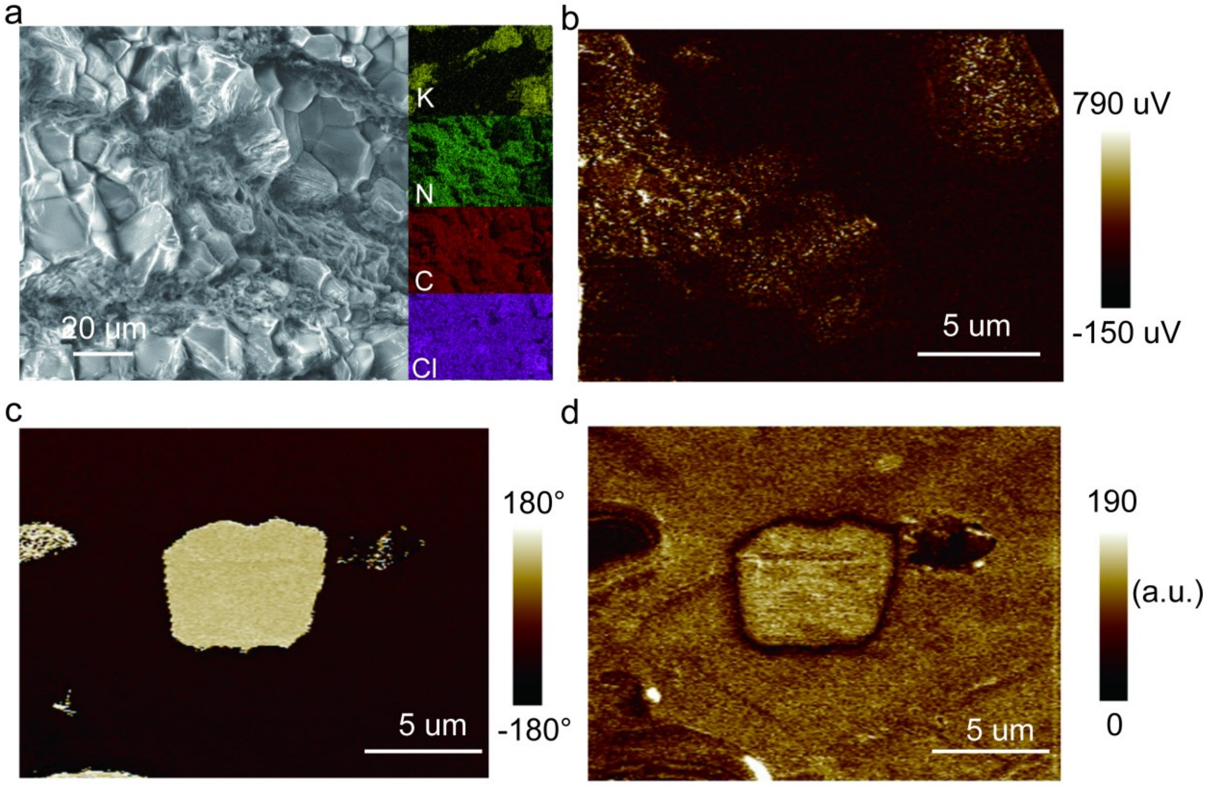

Figure 3

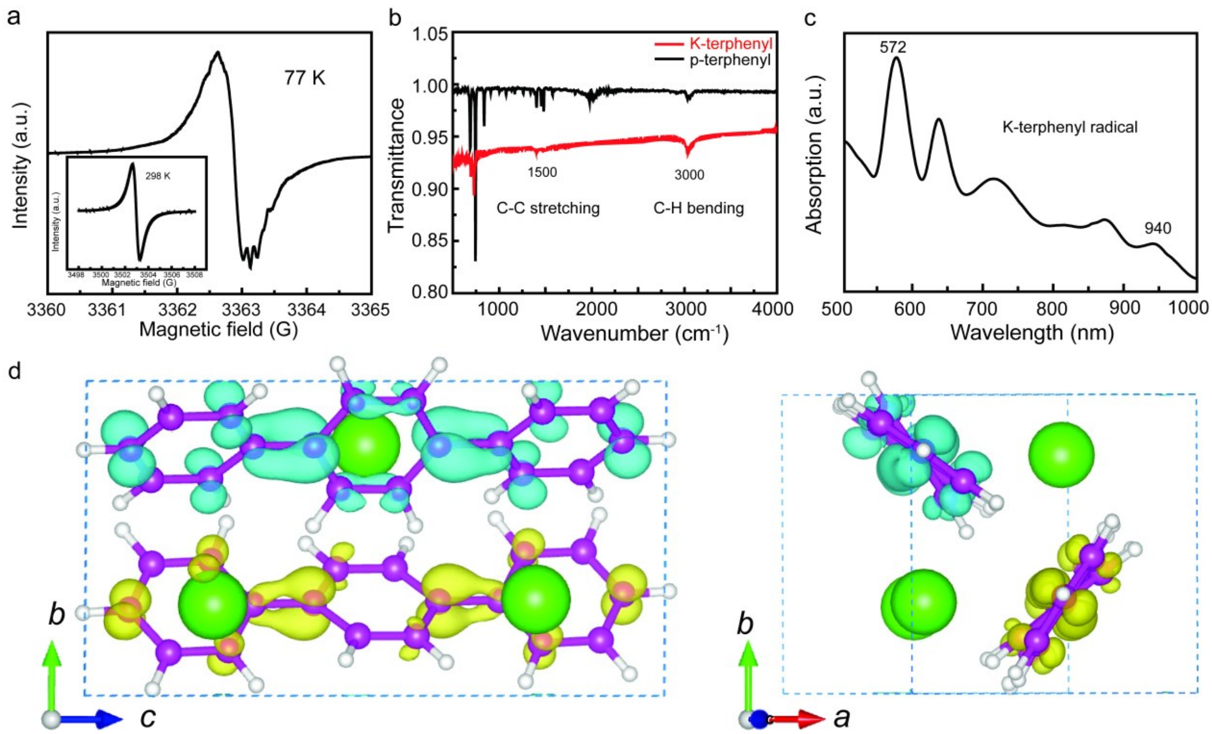

Figure 4

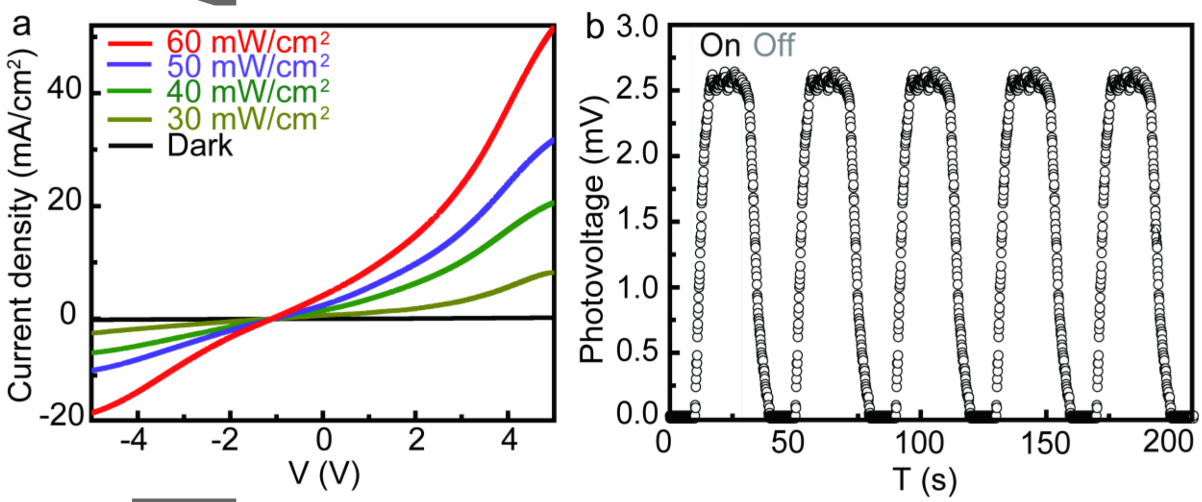

Figure 5

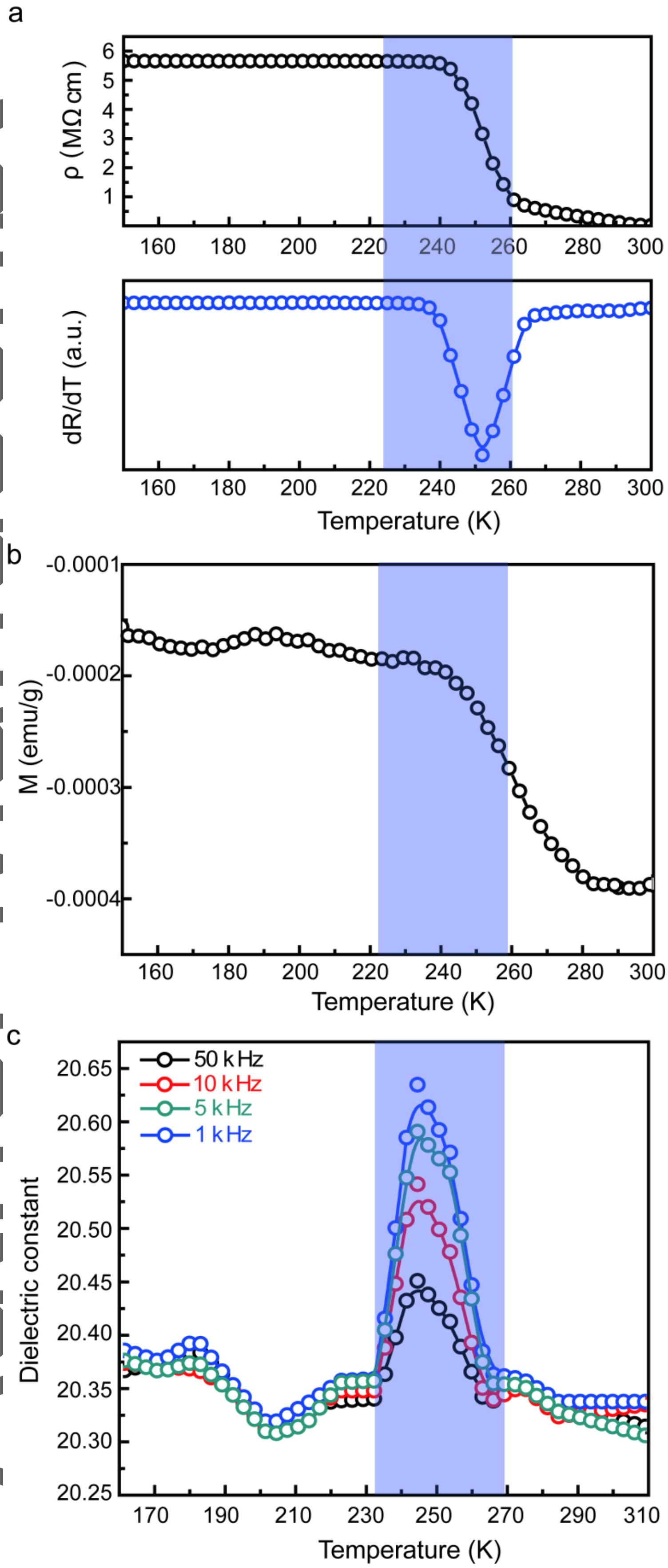
a
ρ (MΩ cm)
dR/dT (a.u.)
Temperature (K)
b
M (emu/g)
Temperature (K)
c
50 kHz
10 kHz
5 kHz
1 kHz
Dielectric constant
Temperature (K)

Figure 6

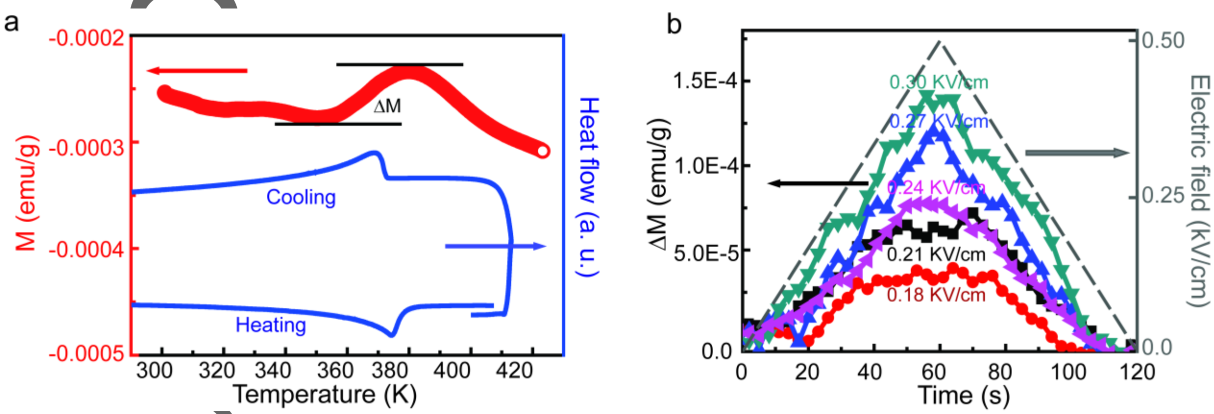

TOC

Ferroelectricity together with magnetic spin exchange coupling were achieved in molecular radical hydrocarbon solids. The ability to simultaneously control and retrieve the changes in magnetic and electrical responses opens up a new breadth of applications, such as radical magnetoelectrics, magnets, and optoelectronics.

Keyword: Molecular radicals, Hydrocarbon, Magnetoelectrics, Ferroelectricity.

Ying-Shi Guan,[1,2] Guohua Zhong,[3] Yong Hu,[1,2] Anthony F. Cannella,[4] Changning Li,[1,2] Namhoon Lee,[1,2] Quanxi Jia,[5] David C. Lacy,[4,] and Shenqiang Ren[1,2,*]*

Magnetoelectric radical hydrocarbons